Catalysis Today 149 (2010) 82–90

Contents lists available at ScienceDirect

Catalysis Today

journal homepage: www.elsevier.com/locate/cattod

Investigation into the effect of the intermediate carbon carrier on the catalytic activity of the HDS catalysts prepared using heteropolycompounds

P.A. Nikulshin [a], N.N. Tomina [a], A.A. Pimerzin [a], A.V. Kucherov [b], V.M. Kogan [b,*]

[a] Samara State Technical University, 244 Molodogvardiyskaya St., Samara 443100, Russia
[b] N.D. Zelinsky Institute of Organic Chemistry, RAS, 47 Leninsky Prosp., Moscow 119991, Russia

ARTICLE INFO

Keywords:
Hydrotreatment
Catalysis
Carbon
Intermediate support
Heteropolycompounds
Diesel
Activity
Benzene
Thiophene

ABSTRACT

The effect of the intermediate activated carbon covering the alumina carrier on catalytic activity of the supported transition metal sulfides (TMS) prepared from heteropolycompounds (HPCs) in thiophene hydrodesulfurization (HDS), benzene hydrogenation (HYD) and hydrotreating (including HDS of S-containing and HYD of polyaromatic compounds) of diesel oil fractions was investigated. Carbon content on the alumina carrier varied from 0 to 3.8 wt.%. It was found that the structure of carbon coating the alumina surface changes depending on the presence/absence of the active phase on the intermediate activated carbon. Total catalytic activity of the catalysts in HDS and HYD reactions was maximal for carbon content of 1–2 wt.% and fell down for catalysts with 3.8 wt.% of carbon. The specific catalytic activity grew proportionally to the carbon content on the catalyst. The experimental data showed that a rise of the reaction temperature leads to a decrease in the amount of adsorbed hydrogen whose deficiency limits the formation of H_2S. It was supposed that the intermediate carbon placed between the alumina carrier and the active phase accumulates hydrogen inside carbon pores. Besides, the intermediate C-carrier of the catalysts synthesized from Co(Ni) salts of heteropolycompounds promotes rising of stacking number in nanoslabs of the active CoMoS phase of the second type.

1. Introduction

Recently HPCs have been widely used as precursors of the active phase of HDS catalysts. Heteropolycompounds are complex inorganic compounds formed by Mo (or (and) W) atoms and central atoms named heteroatoms. Different types of HPCs with Keggin [1–15] or Anderson [14–25] structures were also proposed as starting materials for the preparation of hydrotreating catalysts. One of the reasons for a high activity of the catalysts synthesized from the HPCs of Anderson structures may be synergetic effect between the atoms of the promoter and the main active compound [14,24–26] because they are introduced onto the catalyst surface from one molecule. In our previous works [15,22,23] we used Anderson type of HPCs with central elements of 3d-metals as precursors of hydrotreating catalysts and observed essential improvement of catalytic properties of these catalysts as compared to conventionally prepared samples.

According to Breysse et al. [27], carrier nature much affects catalysts activity. Mazurelle et al. [26] reported that the catalysts prepared on the basis of HPC and supported on alumina, titania or zirconia considerably differ in their catalytic activities. The highest catalytic activity was observed on the catalysts supported on alumina but the use of TiO_2 and ZrO_2 did not improve catalyst activity in hydrotreating.

At the same time, C-supported catalysts are more active than alumina supported [28,29]. Carbon-supported catalysts show many advantages: high specific surface area, controlled pores structure and surface properties, weak interaction with active phase precursor and some others. However, charcoal has some shortcomings, narrow pore structure inaccessible to large molecules containing sulfur and low bulk density among them. To overcome these shortcomings, we decided to cover alumina with activated carbon and thus to prepare a catalyst with an intermediate support between the alumina and active phase. A few attempts to increase catalytic activity by depositing active carbon on alumina and to explain the positive effect of deposited carbon on catalytic activity were made before [30,31]. However, systematic studies of this effect were not carried out.

In the given paper we report the results of synthesis and characterization of the C-coated alumina carriers and the catalysts prepared using these supports and the $NiMo_6$- and Co_2Mo_{10}-HPCs and of their catalytic activities in benzene hydrogenation, thiophene hydrodesulfurization and hydrotreating of diesel fraction.

* Corresponding author at: N.D. Zelinsky Institute of Organic Chemistry, Russian Academy of Sciences, Radioisotopic Research Group, 47 Leninsky Prospect, 119991 Moscow, Russia. Tel.: +7 499 1358910; fax: +7 499 1355328.
E-mail addresses: vmk@ioc.ac.ru, kogan@gagarinclub.ru (V.M. Kogan).

0920-5861/$ – see front matter © 2009 Elsevier B.V. All rights reserved.
doi:10.1016/j.cattod.2009.11.016

2. Experimental

2.1. Materials, their synthesis and characterization

The ammonium salts of 6-molybdonickelate $(NH_4)_4[Ni(OH)_6Mo_6O_{18}]\cdot 5H_2O$ (here in $NiMo_6$) and decamolybdodicobaltate(III) $(NH_4)_6[Co_2Mo_{10}O_{38}H_4]\cdot 7H_2O$ (here in Co_2Mo_{10}) heteropolyacids were synthesized in accordance with published procedures [32,33]. To confirm the structure of the heteropolycompounds, their IR spectra were recorded and phase composition was determined. The IR spectra of crystalline HPCs predried at 110 °C and pelletized with KBr were recorded on an Avatar-360 (FTIR). The phase composition of the synthesized HPCs was determined on a DRON-2 X-ray diffractometer (Cu anode, K_α radiation).

Synthesis of C-contained carriers $C_x/\gamma\text{-}Al_2O_3$ (x = 1.2, 2.3, 3.8 wt.%) was carried out by pyrolysis of organic compounds on alumina in a bench-scale flow reactor at 600 °C in N_2 atmosphere during 1.5–2 h. The coke contents of spent catalysts were determined by quantitative oxidation to CO2 followed by GC analysis.

The texture characteristics of the prepared carriers were determined by nitrogen adsorption at 77 K on a Micromeritics ASAP 2020 adsorption porosimeter. The specific surface area was calculated using the BET method at a relative partial pressure of P/P_0 = 0.2. The total pore volume and pore size distribution were determined by an adsorption curve using the Barrett–Joiner–Halenda model at a relative partial pressure of P/P_0 = 0.99.

Ni_2–$NiMo_6/C_x/\gamma\text{-}Al_2O_3$ catalysts were prepared by means of the incipient wetness technique via impregnating the support ($\gamma\text{-}Al_2O_3$ or $C_x/\gamma\text{-}Al_2O_3$) with $NiMo_6$ and $Ni(NO_3)_2$ solutions. For Co_3–$Co_2Mo_{10}/C_x/\gamma\text{-}Al_2O_3$ catalysts we used the joint solution of Co_2Mo_{10} и $Co(NO_3)_2\cdot 6H_2O$. The calculated amounts of MoO_3 and NiO in the catalysts were 16 and 4 wt.%, respectively. The samples were dried at 80, 100, and 120 °C and calcined at 400 °C for 2 h. C-contained catalysts were dried and calcined in N_2 atmosphere. The catalysts were sulfidized by H_2S/H_2 at 400 °C during 2 h.

The C-contained carriers were studied by combined TG-DTG-DTA method using the derivatograph C (“MOM”) under the conditions: linear heating up to 650 °C in the alundum crucibles with the heating rate of 10 °C/min in air. The $\alpha\text{-}Al_2O_3$ was used as references.

The ESR-spectra were taken in the X-band ($\lambda \cong 3.2$ cm) at 20 and −196 °C on a reflecting spectrometer, equipped with a co-axial quartz Dewar. The ESR signals were registered in the lack of saturation in the field range of 0–4700 and 3100–3500 G. DPPH was used as a reference. The samples were placed in identical glass ampoules (2.0 mm diameter, 20 mm height), evacuated for 2–3 min at 90–100 °C to ∼0.1 Torr, and sealed off. Then the ESR-spectra were registered, ampoules were open to air, and ESR measurements were repeated immediately. The presence of carbon residue in the catalysts caused a considerable sensitivity drop due to the absorption of microwave power, so only small charges of sample placed into thin ampoules could be used for correct measurements.

HRTEM images of the catalysts were obtained on a JEM-2010 electron microscope (JEOL, Japan) with a lattice-fringe resolution of 0.14 nm at an accelerating voltage of 200 kV. The high-resolution images of periodic structures were analysed by the Fourier method. Local energy-dispersive X-ray analysis (EDX) was carried out on an EDAX spectrometer (EDAX Co) fitted with a Si (Li) detector with a resolution of 130 eV. The samples examined by HRTEM were prepared on a perforated carbon film mounted on a copper grid.

2.2. Catalytic activity examination

2.2.1. Thiophene hydrodesulfurization

The catalytic activity of the samples in thiophene HDS was measured in a pulse microcatalytic system at 360 °C and atmospheric pressure. The catalyst loading was 25 ± 1 mg, and the volume of thiophene was 0.2 μL. The reaction products were analysed using GC with the separation of the compounds on OV-101 silica capillary column and detecting by the PID. We measured stationary activity of the catalysts after 20 thiophene injections.

2.2.2. Benzene hydrogenation

The model structurally insensible reaction of benzene hydrogenation was used for HYD activity testing (P_{H_2} = 2.0 MPa, a reaction temperature range was between 300 and 460 °C, flow conditions). Catalyst loading was 0.450 ± 0.005 g. Particle size was 0.25–0.5 mm. Hydrogen flow velocity was 40 cm^3/min, benzene feed rate was 0.5 mL/h. Hydrogen and benzene were mixed in a mixer-evaporator. After that the benzene–hydrogen mixture was fed into the reactor. The products were injected through a 6-way valve-sampler equipped with a loop of 1 μL into the GC installed at the outlet of the reactor. GC analysis was carried out using a stainless steal column filled by sorbent containing 15 wt.% Carbowax 20M on Chesosorb with graining of 0.25–0.36 mm. He was used as carrier gas. The benzene conversion in all the experiments was less than 18%. Cyclohexane and traces of methylcyclopentane (<1 wt.%) were formed in the products.

2.2.3. Hydrotreating of diesel fraction

The synthesized catalysts were tested in a bench-scale flow reactor unit in the process of hydrotreating 20:80 mixture (by volume) of light catalytically cracked gas oil and straight-run diesel. The sulfur content of the feedstock was 1.134 wt.%, and the amount of polycyclic aromatic compounds (PACs) was 4.83 wt.%. The system contained units for specifying, maintaining, and controlling the temperature, pressure, and hydrogen-containing gas and feed flow rates. The reactor temperature, pressure, and feed and hydrogen flow rates were maintained within ±2 K, ±0.05 MPa, ±0.2 ml/h, and 0.2 l/h, respectively. The tests were performed under the following conditions: temperatures of 320, 340, 360, and 380 °C; pressure of 4.0 MPa; feed volume space velocity of 2.0 h^{-1}; hydrogen: feedstock ratio of 600 Nl/l; and catalyst volume of 10 cm^3. The total sulfur contents of the feed and hydrogenation products were determined on a EDX800HS Schimadzu analyser, and the concentrations of polycyclic aromatic compounds were determined on a Shimadzu UV-1700 spectrophotometer.

Catalysts activity was determined under the remanent amount of sulfur (HDS) and PACs (HYD) in hydrogenation products.

$$\mathrm{HDS} = \frac{C_S^0 - C_S}{C_S^0},$$

C_S^0 – sulfur content in feedstock, 1.134 wt.%; C_s – sulfur content in hydrogenation products, wt.%.

$$\mathrm{HYD} = \frac{C_{PACs}^0 - C_{PACs}}{C_{PACs}^0},$$

C_{PACs}^0 – PACs content in feedstock, 4.83 wt.%; C_{PACs} – PACs content in hydrogenation products, wt.%.

3. Results

3.1. Characteristics of the $NiMo_6$ and the Co_2Mo_{10}

The FTIR spectra of synthesized $NiMo_6$ and Co_2Mo_{10} are given in Fig. 1. The characteristic bands of the $NiMo_6$ of the Anderson type

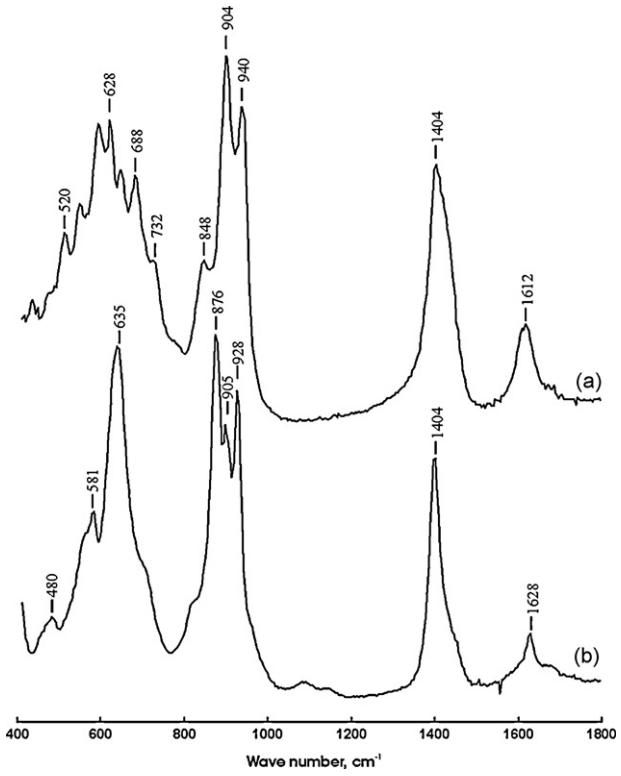

Fig. 1. The FTIR spectra of (a) Co2Mo10-HPC and (b) $NiMo_6$HPC after drying at 110 °C.

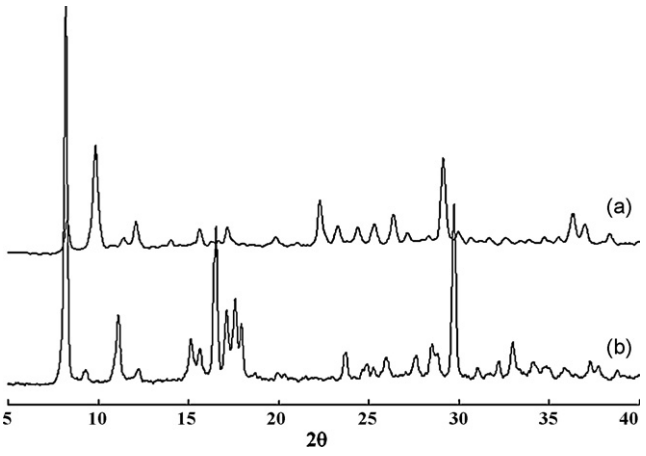

Fig. 2. The XRD spectra of (a) Co2Mo10-HPC and (b) $NiMo_6$HPC after drying at 110 °C.

coincide with the characteristic bands described in [24,34–36]. Intensive absorption bands in the area of 950–880 cm^{-1} correspond to *cis*-MoO_2-bonds, the absorption bands in the area of 650–450 cm^{-1} correspond to Mo–O–Mo bridge bonds. In the range of 1400–1600 cm^{-1} the deformation vibrations of NH_4^+ and H_2O were observed. Co_2Mo_{10} is a derivative composition from the Anderson structure [36]. The IR spectra of the Co_2Mo_{10} contain replicas similar by their intensities to the IR spectra of the $NiMo_6$ and correspond to the spectra described in [24]. The XRD analysis of the $NiMo_6$ and Co_2Mo_{10} indicates a complex crystalline structure of these compounds (Fig. 2). Besides, their interplanar distances coincide with the earlier described distances for these HPCs [20,37,38].

3.2. Textural characteristics of the prepared C-contained alumina carriers

The prepared C-containing carriers differ by their textural characteristics from each other (Table 1). Carburizing of the pores of γ-Al_2O_3 by coke led to a decrease in the specific surface of the prepared carriers as compared to initial alumina. The average pore diameter increased while the total pore volume diminished. These results can be explained by blocking of the micropores (their contribution into the total value of the specific surface is essential) by coke formed on the alumina surface. It is a reason for an observed increase in an average diameter of the pores of the carrier. Comparison of the textural characteristics of $C_{1.2}$/γ-Al_2O_3 and $C_{2.3}$/γ-Al_2O_3 carriers (1.2 and 2.3 wt.% of carbon on alumina, respectively) shows a small rise of the specific surface and slope opposition for the average pore diameter at the constant total pore volume of a carrier at a double increase in the amount of the coating carbon. Increase of carbon content affects pore volume distribution (Fig. 3). It means that the deposed coke is distributed on the surface of γ-Al_2O_3 not as a monolayer. Further increase in coke content up to 3.8 wt.% essentially reduces the specific surface area and pore volume of the carrier.

3.3. TG-DTG-DTA measurements of the carriers

DTA analysis of the C-contained carriers in air showed (Fig. 4a) that oxidation of the surface carbon was accompanied by a typical exothermic effect and was observed at $T \geq 300$ °C. Maximal exothermic effect for the C-containing carriers was within 409–412 °C. The DTG plots of the obtained carriers (Fig. 4) indicate that oxidation process for the $C_{3.8}$/γ-Al_2O_3 is not over even at 600 °C, *i.e.* the C-deposition formed is high-temperature coke.

3.4. ESR analysis of the C_x/γ-Al_2O_3 carriers and prepared catalysts

The samples of C_x/γ-Al_2O_3 carriers and Ni–Mo catalysts supported on them were studied by ESR. No broad ESR lines typical of isolated or weakly interacting Mo^{5+} ions were detected in all the catalysts under study (fresh, sulfided or used). Only narrow symmetric singlets ($g = 2.003$; $\Delta H < 10$ G) were registered, typical of the "coke" residue in the samples.

3.4.1. ESR analysis of the C_x/γ-Al_2O_3 carriers (x = 1.2, 2.3 and 3.8 wt.%)

The evacuated samples of carbon-containing supports show narrow intense ESR lines with $g = 2.003$ and $\Delta H \cong 5$–6 G, and inlet of air causes a drastic decrease in the ESR line intensity with some line broadening. A resulting drop in the signal integral intensity reaches ~2 orders of magnitude, as Fig. 5 illustrates for the sample

Table 1
Composition and textural characteristics of the initial γ-Al_2O_3 and the prepared carriers.

No.	Carrier	Carbon content (wt.%)	BET Surface area (m^2/g)	Pore volume (cm^3/g)	Average pore diameter (Å)
1.	γ-Al_2O_3	–	169	0.679	118
2.	$C_{1.2}$/γ-Al_2O_3	1.2	132	0.622	138
3.	$C_{2.3}$/γ-Al_2O_3	2.3	145	0.621	130
4.	$C_{3.8}$/γ-Al_2O_3	3.8	104	0.448	144

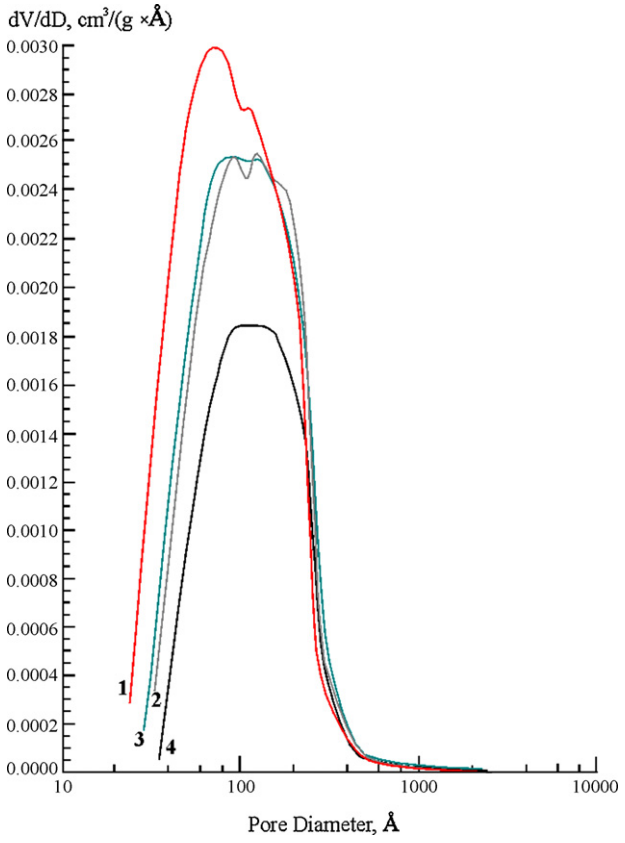

Fig. 3. Plots of the pore volume distributions of the carriers: 1, γ-Al_2O_3; 2, $C_{1.2}$/γ-Al_2O_3; 3, $C_{2.3}$/γ-Al_2O_3; 4, $C_{3.8}$/γ-Al_2O_3.

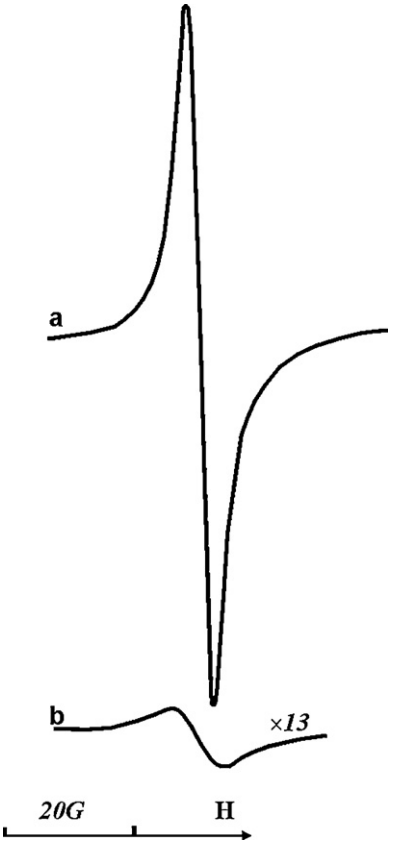

Fig. 5. The ESR signal, taken at 20 °C, from the coked support, $C_{3.8}$/γ-Al_2O_3: (a) evacuated (~0.1 Torr); (b) exposed to air (magnification factor 13×). The integral intensity changed by a factor of ~33; g = 2.003.

with 3.8 wt.% of C. This strong effect caused by O_2 presence in the gas phase is typical for so-called "high-temperature" carbons with a considerable degree of graphitization (polyaromatics formation). The result obtained seems to be appropriate since the carbonated support was pre-calcined at 600 °C for a long time upon preparation.

3.4.2. ESR analysis of the oxide Ni_2–$NiMo_6$/C_x/γ-Al_2O_3 catalysts

Narrow ESR lines of the same type typical for the coke residue are preserved for as-made oxide catalysts but become considerably less intense for the supported catalysts prepared by impregnation with subsequent calcination of the samples in inert atmosphere. In addition, the dependence of the signal intensity from air presence becomes considerably less pronounced: air inlet on evacuated samples causes only 2–3-fold drop of the integral intensity (Fig. 6). Such a weak effect of O_2 presence is indicative of the amorphous nature of the coke with considerably reduced graphitization level.

Thus, catalyst preparation, in spite of relatively low treatment temperature, is accompanied by both partial loss of the carbon and amorphization of the remaining part of the coke. This quite interesting result is indirect evidence that the coke of the starting support (being formed at 600 °C) takes part in further steps of the active phase forming upon calcination of supported Ni_2–$NiMo_6$/C_x/γ-Al_2O_3 at temperature as low as 400 °C.

3.4.3. ESR analysis of the sulfidized Ni_2–$NiMo_6$/C_x/γ-Al_2O_3 catalysts and spent catalysts after hydrotreating of diesel faction

Sulfidizing of the oxide Ni_2–$NiMo_6$/C_x/γ-Al_2O_3 precursors is not accompanied by any measurable change of the "coke"-ESR signal either by intensity or sensitivity to air exposure (Fig. 7). Catalytic testing of the sulfided Ni_2–$NiMo_6$(S)/C_x/γ-Al_2O_3 samples in diesel fraction hydrotreatment results in a measurable increase of the

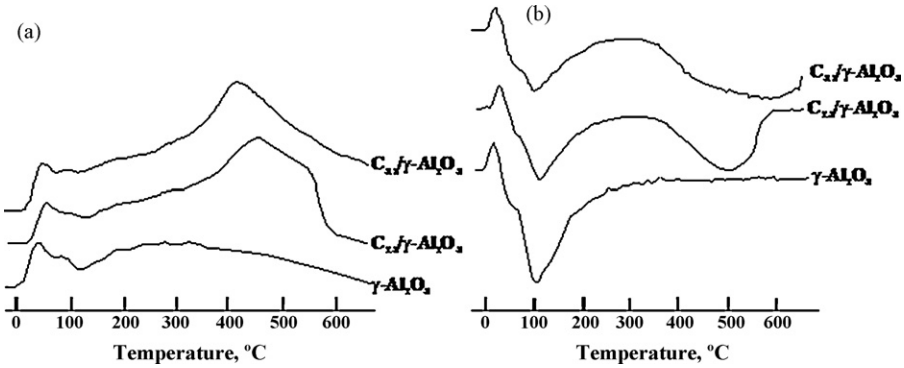

Fig. 4. The plots of (a) DTA and (b) DTG of the prepared carriers.

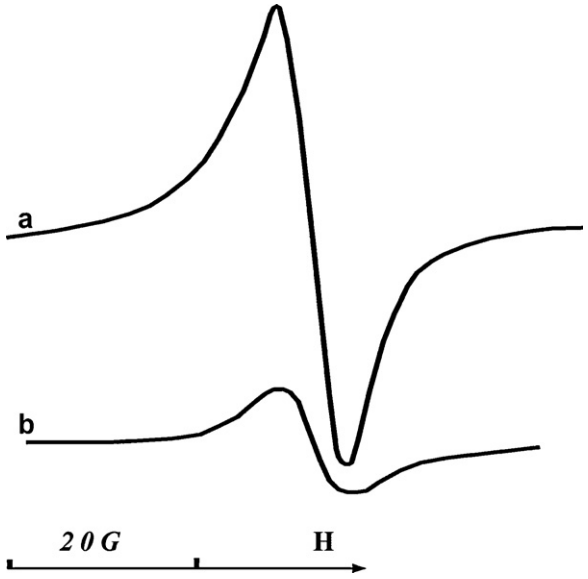

Fig. 6. The ESR signal, taken at 20 °C, from the sample Ni_2–$NiMo_6/C_{2.3}/\gamma$-Al_2O_3: (a) evacuated (~0.1 Torr); (b) exposed to air (identical magnification). The integral intensity changed by a factor of ~2.4; $g = 2.003$.

"coke"-ESR signal integral intensity. However, the signal demonstrates the same relatively low sensitivity to air exposure (Fig. 7). Thus, additional accumulation of coke seems to take place without any considerable graphitization of the residue.

3.4.4. ESR analysis of the Ni_2–$NiMo_6/Al_2O_3$ catalysts

Ni_2–$NiMo_6/\gamma$-Al_2O_3 reference catalyst (supported on non-coked alumina) shows no ESR signals after calcination and sulfidizing steps. The sample after hydrotreatment catalytic testing shows a very weak narrow ESR line with low sensitivity to air exposure typical of amorphous (low-temperature) coke residue.

3.5. HRTEM analysis of the catalysts

The HRTEM pictures of sulfided catalysts are presented in Fig. 8. The average length of the slabs in the active phase of the Co_3–Co_2Mo_{10}/Al_2O_3 sulfide catalyst is 3.5 nm and the average stacking number is 2.6. Thus, the high activity of the Co_2Mo_{10}-HPC based catalysts can be explained by the formation of the CoMoS-II phase [39]. In Payen and co-workers [25] reported that the average length of the MoS_2 slabs of the catalyst prepared also from Co_2Mo_{10}-HPC was 2.8 nm and the average stacking number was 1.7. The difference in the stacking number (greater in our samples) may be related to different regimes of sulfidation, textural and acid-based characteristics of carriers. The HRTEM data of the Co_3–$Co_2Mo_{10}/C_{1.2}/Al_2O_3$ catalysts showed that the average length of the slabs was 3.1 nm, which is a bit less than for Co_3–Co_2Mo_{10}/Al_2O_3 catalyst. At the same time, the average stacking number in multilayer slabs increased from 2.6 up to 2.9.

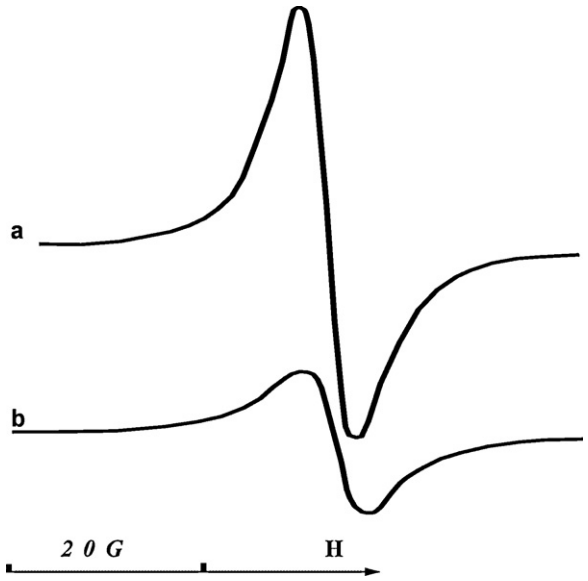

Fig. 7. The ESR signal, taken at 20 °C, from the used Ni_2–$NiMo_6(S)/C_{3.8}/\gamma$-Al_2O_3: (a) evacuated (~0.1 Torr); (b) exposed to air (identical magnification). The integral intensity changed by a factor of ~1.8; $g = 2.003$.

3.6. Catalytic activity examinations

3.6.1. Thiophene hydrodesulfurization

For the catalysts supported on the $C_{3.8}/Al_2O_3$ the HDS activity reduced as compared to the catalysts without carbon. It can be explained by a decrease in the active phase dispersity induced by a fall of the specific surface area (Fig. 9). The dependence of HDS activity from C-content in the carrier passes through the maximum and the catalysts containing 1.2–2.3 wt.% of carbon exhibit maximal HDS activity. This regularity does not depend on the nature of the catalyst precursor and is correct both for $NiMo_6$- and for Co_2Mo_{10}-based catalysts.

3.6.2. Benzene hydrogenation

The rates of benzene hydrogenation were measured in the course of stepped temperature increases within the whole temperature range (300–460 °C, a step value was 20 °C) at steady benzene conversion (after every 1 h since stabilizing of benzene conversion at current temperature). Benzene conversion was as well measured when the reaction temperature went down. In both methods of measurements the kinetic curves were fully reproduced. The measurements of catalytic activity of every catalyst sample were repeated several times but during the experiments no noticeable decrease in catalytic activity was observed.

The dependences of the rates of benzene HYD over sulfide Ni_2–$NiMo_6$ catalysts are given in Arrhenius plots (Fig. 10). It is seen that in the experimental temperature range all the dependences have the inflection points (for Ni_2–$NiMo_6/\gamma$-Al_2O_3 – at 340 °C; for Ni_2–$NiMo_6/C_{2.3}/\gamma$-Al_2O_3 – at 360 °C; for Ni_2–$NiMo_6/C_{3.8}/\gamma$-Al_2O_3 – at 380 °C). The examination of HYD activity showed similar activities of the Ni_2–$NiMo_6/C_{2.3}/\gamma$-Al_2O_3 and Ni_2–$NiMo_6/\gamma$-Al_2O_3 catalysts. In contrast, the Ni_2–$NiMo_6/C_{3.8}/\gamma$-Al_2O_3 exhibited lower activity.

3.6.3. HDS of diesel faction

The results of the testing of the prepared catalysts in hydrotreating of diesel fraction are given in Figs. 11 and 12. As seen in Fig. 11, the highest HDS activity was for the catalysts with 2.3 wt.% of carbon on alumina. The catalyst containing 1.2 wt.% of carbon is less active than Ni_2–$NiMo_6/C_{2.3}/\gamma$-Al_2O_3 catalyst. The lowest HDS activity was exhibited by the catalyst containing 3.8 wt.% of coke on alumina even as compared to the non-containing coke catalyst Ni_2–$NiMo_6/\gamma$-Al_2O_3. The HYD activity in the course of diesel hydrotreating reduces in the following order: $C_{1.2}/Al_2O_3 > C_{2.3}/Al_2O_3 = Al_2O_3 > C_{3.8}/Al_2O_3$.

In the series of the Co–Mo catalysts (Fig. 12a) the highest activity was demonstrated by the sample with 1.2 wt.% of carbon on alumina. Catalysts with 2.3 and d 3.8 wt.% of carbon, were considerably less active in the HDS of diesel fraction. Catalyst without carbon on alumina demonstrated intermediate activity between the catalyst with 1.2 wt.% of carbon and the others. A change of the HYD activity with carbon content on alumina (Fig. 12b) is symbate with HDS activity for the Co–Mo

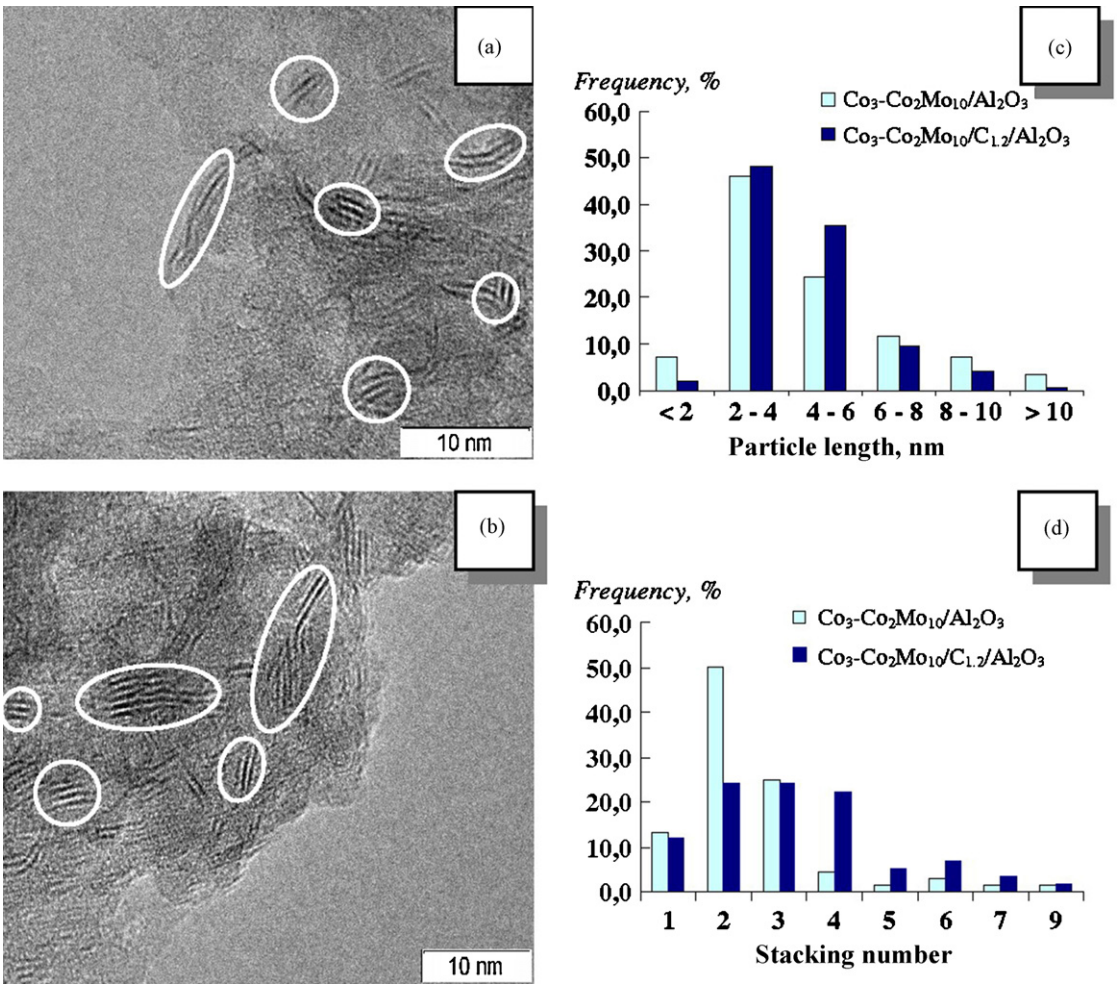

Fig. 8. HRTEM micrographs of sulfided catalysts (a) Co_3–Co_2Mo_{10}/γ-Al_2O_3, (b) Co_3–Co_2Mo_{10}/$C_{1.2}$/γ-Al_2O_3 and the distributions of slab lengths of MoS_2 particles (c) and of stacking number of MoS_2 particles (d).

catalysts and can be presented in the order: $C_{1.2}/Al_2O_3 > C_{2.3}/Al_2O_3 > Al_2O_3 > C_{3.8}/Al_2O_3$.

4. Discussion

Benzene HYD and thiophene HDS is a model reaction for hydrotreating processes of various oil fractions. An essential fall of HYD and HDS rates for the catalyst with 3.8 wt.% of carbon as compared to the catalysts with 0 and 2.3 wt.% of carbon can be explained by the lowest surface square of the carrier for $C_{3.8}$/γ-Al_2O_3 sample (Table 1) and, possibly, of the active surface of the catalyst. The observed decrease in the surface area of the carrier for $C_{2.3}$/γ-Al_2O_3 sample as compared to pure alumina is likely to be compensated by less interaction between the active phase and the carrier. According to [39], the interaction of the "CoMoS" phase with alumina results in the formation of the Al–O–Mo bonds which reduce the catalytic activity of the active phase. It is likely that coke presence in the form of the intermediate support between the

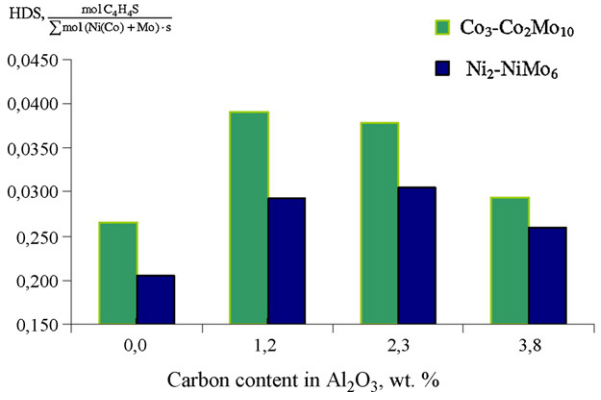

Fig. 9. HDS activity in thiophene hydrogenolysis at 360 °C of the catalysts prepared on the basis of $NiMo_6$ and Co_2Mo_{10}, supported on Al_2O_3 and C/γ-Al_2O_3.

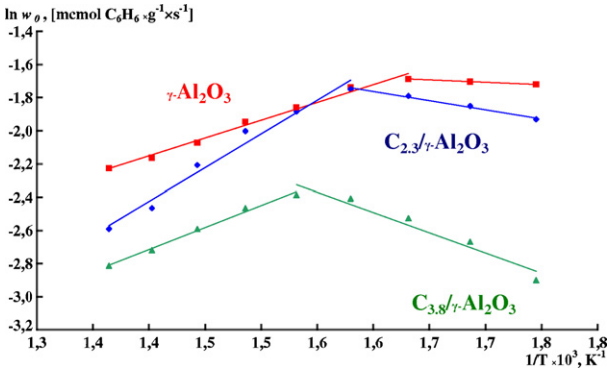

Fig. 10. The temperature dependencies of the rate of the benzene hydrogenation rate for the Ni_2–$NiMoG_6$/C_x/γ-Al_2O_3 catalysts with various (different) carbon content in Arrhenius plots.

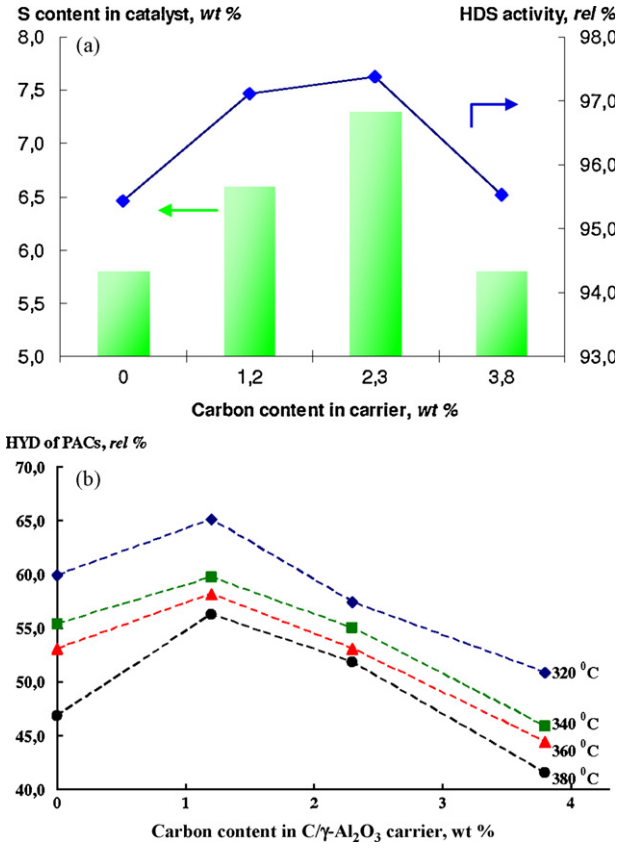

Fig. 11. (a) HDS activity and sulfur content in the sulfided Ni_2–$NiMo_6/C_x/\gamma$-Al_2O_3 catalysts and (b) HYD activity in the course of the polyaromatics hydrogenation on these catalysts vs. deposited carbon content on the alumina carrier.

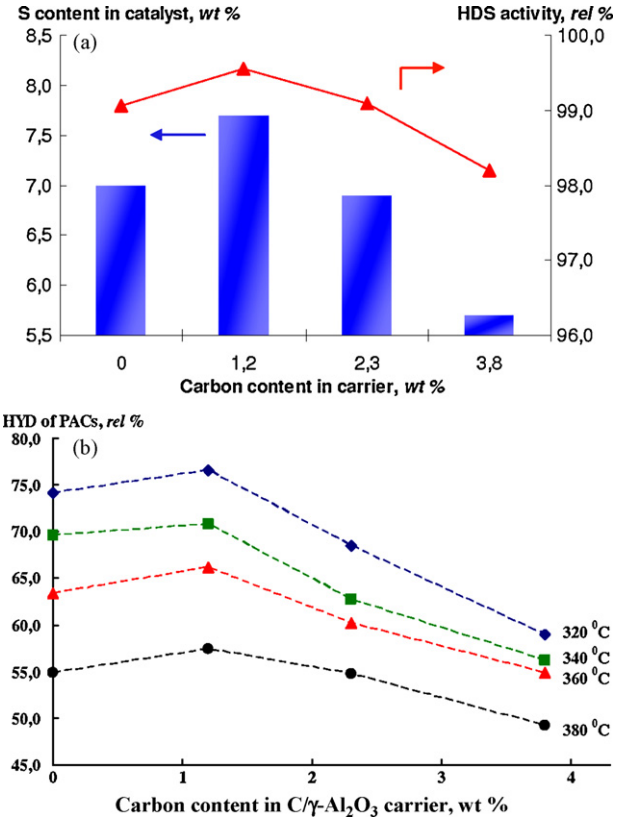

Fig. 12. (a) HDS activity and sulfur content in the sulfided Co_3–$Co_2Mo_{10}/C_x/\gamma$-Al_2O_3 catalysts and (b) HYD activity in the course of the polyaromatics hydrogenation on these catalysts vs. deposited carbon content on the alumina carrier.

active phase and alumina prevents the formation of such bonds. The use of the C-covered Al_2O_3 with carbon content 1.2 wt.% ($C_{1.2}/Al_2O_3$) as a catalyst support leads to an increase in the average stacking number in the MoS_2 slabs (Fig. 8). Such a substantial change of the active phase morphology is probably determined by weakening of the interaction of the active phase and the support due to an effect of the intermediate carbon support covering the main Al_2O_3 carrier.

The temperature dependences in Arrhenius plots (Fig. 10) show that the benzene HYD rates fall down and the inflexion points shift to the high-temperature area with an increase of the carbon content in the catalysts.

Our data show that with an increase in carbon content the specific surface area of the prepared carriers decreases (Table 1). So, the dispersity of the active phase and the number of the active sites should fall down. This is likely to be a reason of decrease in HYD rate of benzene.

The shape of the kinetic curves can hypothetically be explained by these reasons: (i) by thermodynamic limitations because the benzene hydrogenation reaction is largely exothermic, (ii) by irreversible catalyst deactivation and (iii) by reversible catalyst deactivation.

The first explanation (thermodynamic limitations) should be declined because the reaction rates were measured at low benzene conversions (Section 2.2.2) and the reached composition of the product mixture was far from the product composition corresponding to the equilibrium state [39].

The second explanation (irreversible deactivation of the catalyst) should also be declined because the catalysts activity in steady state was measured both at increasing and decreasing reaction temperatures and the curves behavior was found to be reversible. In addition, as it was shown by Startsev et al. [40,41], the temperature dependence of benzene hydrogenation rate passes through the maximum that is not determined by catalyst deactivation or transition of the reaction into the diffusion region.

The third explanation (reversible catalyst deactivation) remains to be discussed. Reversible deactivation of the catalyst is conditioned by limiting of the reaction rates by either adsorbed benzene or adsorbed hydrogen. Because the constant of hydrogen adsorption is less than that of adsorption of benzene, the observed inflation point is determined by hydrogen accumulation. This agrees with the data reported by Romero et al. [42] for supported NiMo sulfides, the limiting step of hydrogenation is concentration of adsorbed hydrogen. The ability of carbon adsorbents and C-supported sulfide catalysts to store hydrogen is widely known [43 and references within it].

When the reaction temperature rises, the amount of adsorbed hydrogen decreases and its deficiency limits the formation of the H_2S. Possibly, carbon intermediate support accumulates molecular hydrogen in the pores or cavities of the inert amorphous carbon layer without dissociation. This hydrogen is needed for the interaction with the catalyst SH groups. The interaction results in the H_2S formation. Then the H_2S desorbs into the gas phase and a new vacancy is formed. This explanation fully agrees with the previous data [44]: in the course of the radioisotopic investigations of temperature effects on the number and reactivity of active sites of $CoMoS/Al_2O_3$ catalysts the growth of active site productivities of the catalysts is limited by the amount of adsorbed hydrogen that plays a key role in the HDS reaction. At the reaction temperature the amount of H_2 adsorbed on the catalyst drops down and its deficiency limits the active site productivity.

ESR data (Figs. 5 and 6) demonstrate qualitative transformations of the starting coke residue at different steps of catalyst preparation (impregnation/calcination). In spite of a relatively low

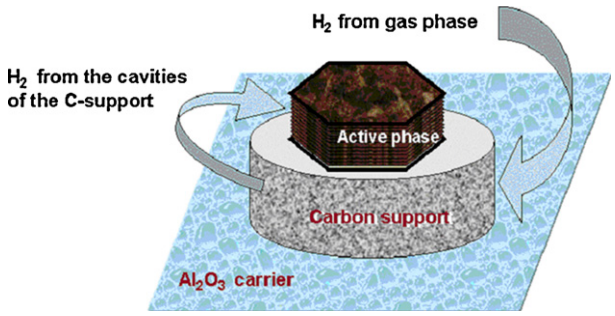

Fig. 13. The proposed model of the role of the intermediate carbon support placed between the active phase and the main carrier.

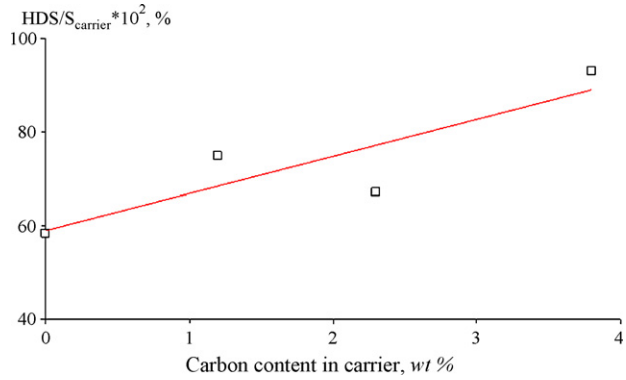

Fig. 14. Dependence of specific HDS activity of the $Co_2Mo_{10}/C_x/\gamma$-Al_2O_3 catalysts vs. content of the deposited carbon.

treatment temperature, both partial loss of the carbon and amorphization of the remaining part of the coke take place. Transformation of the coke morphology indicates that the coke of the starting support takes part a further steps of the formation of the active phase upon calcining of supported Ni_2–$NiMo_6/C_x/\gamma$-Al_2O_3 at 400 °C. It is known [43, p. 678] that C-containing carriers are able to consume noticeable amount of hydrogen and, according to the TPD data, to store it even at high temperature. It is possible that carbon intermediate support between alumina and active phase exhibits these properties (Fig. 13).

The catalytic activity of the Ni_2–$NiMo_6/C_x/\gamma$-Al_2O_3 catalysts in HDS and HYD reactions depends on the content of the carbon deposited on a carrier (Fig. 11). In these catalysts HDS activity correlates with sulfide sulfur content. Both values were maximal for the catalyst with 2.3 wt.% of the deposited carbon. At the same time maximal HYD activity was observed for the catalyst with 1.2 wt.% of the deposited carbon.

The HDS and HYD activities of the Co_3–$Co_2Mo_{10}/C_x/\gamma$-Al_2O_3 catalysts depend on the content of the deposited carbon. In contrast to the Ni_2–$NiMo_6/C_x/\gamma$-Al_2O_3 catalysts, these catalysts demonstrate symbasis in the dependencies of the catalytic activity (HYD and HDS) and in the amount of sulfide sulfur from carbon content. Thus, maximal HDS and HYD activities were observed for the catalyst with 1.2 wt.% of the deposited carbon. This sample contained the maximal amount of sulfide sulfur (Fig. 12). Earlier we established correlations between catalyst HDS activity and the amount of mobile sulfur and mobile sulfur reactivity (mobility). A correlation between the amount of sulfide sulfur and catalytic activity was also observed during our studies of the modified hydrotreating catalysts [5,12] and the catalysts prepared from HPCs [15]. In our investigations with radioactive sulfur [44–51] we found that during thiophene HDS catalyst sulfur is replaced by sulfur from thiophene. Some of the sulfur in the sulfide catalyst is "immobile", *i.e.* it cannot participate in the formation of H_2S during the HDS, and some can. The latter can be considered as "mobile". On the basis of these observations we believe that the correlations between catalytic activity and amount of sulfide sulfur can be explained by changes in "mobile" sulfur depending on the amount of the deposited carbon. It seems that the amount of "immobile" part of sulfide sulfur remains constant independently on the amount of deposited carbon.

Increase in the HDS and HYD activities of the catalysts in hydrotreating of diesel oil fraction at some content of deposited carbon of a carrier can be explained in the same way as benzene HYD, namely by reduced interaction between the "CoMoS" phase and carrier and by the deposited carbon ability to accumulate hydrogen and to deliver it to the active sites of the "CoMoS" crystallites in the course of the reaction. High content of the deposited carbon negatively affects catalytic activity, possibly because of the reduction of the specific surface area of the catalysts. However, the catalysts containing the maximal amount of the deposited carbon exhibit the highest specific HDS activity per square of the active surface. Specific HDS activities of the catalysts with 3.8 wt.% of the deposited carbon are considerably higher than specific activities of the rest of the catalysts under study. This is correct both for the Ni_2–$NiMo_6/C_x/\gamma$-Al_2O_3, and Co_3–$Co_2Mo_{10}/C_x/\gamma$-Al_2O_3 catalysts (Fig. 14). No similar dependence for HYD activity was observed for all the catalysts.

It is important that reduction of the specific surface area of the carrier and the supported catalysts with a rise of the carbon deposition leads to the formation of less dispersed active phase. The specific surface of the C-contained catalysts falls down with an increase in the deposited carbon. Hence it is reasonable to expect that a decrease in the dispersion of the CoMoS (NiMoS) active phases intensifies the formation of the CoMoS (NiMoS) phase of type II, *i.e.* multi-layers of the CoMoS (NiMoS) slabs. To explain this phenomenon, we need the "rim-edge" model by Chianelli et al. [52–54] according to which the HDS sites are mostly located on the edges of the CoMoS slab whereas HYD sites are placed on the rims of the slab. It is likely that with an increase in carbon content CoMoS slabs of type II grow in height and remain stable in their diameter because HDS activity increases at constant HYD activity.

The deposited carbon weakens the interaction of the active phase with the carrier, increases sulfur mobility and vacancy formation and thus raises the HDS activity. But at the same time the number of the HDS active sites is reduced due to coating the walls of the slab with the deposited carbon. As the HYD sites are placed on the rims of the slab, they are not subjected to such coating. This model was used in [49] to explain the experimental data of the radioisotopic study of the mechanism of poisoning the active sites with N-containing compounds. We believe that the agreement of the results of [49] with this study supports our explanation.

5. Conclusions

1. Modification of the morphology of the deposited carbon in the course of the synthesis of the TMS catalyst supported on the C-coated alumina shows that the deposited carbon participates in the formation of the active phase.
2. The use of the activated carbon as an intermediate support for the preparation of TMS catalysts increases their HDS and HYD catalytic activities in comparison with the catalysts supported on Al_2O_3.
3. The formation of the intermediate carbon support increases the HDS and HYD activities by weakening interaction of the active "CoMoS" phase of type II and alumina.

Acknowledgements

The authors thank Dr. A.N. Loginova and the members of her team for their assistance in the investigations of the morphology of

the carriers and catalysts, Dr. V.D. Nissenbaum for the DTA-DTG measurements and Dr. V.I. Zaikovsii for the HRTEM analysis of the catalysts.

P. Nikulshin expresses his special gratitude to the Haldor Topsøe A/S Company for the grant on performance of his Ph.D. work (2008–2010).

The work was supported by Russian Federal target program "The scientific and pedagogical staff of innovative Russia".

References

[1] A.A. Spojakina, B. Gigov, D.M. Shopov, React. Kinet. Catal. Lett. 19 (1982) 11.
[2] A.A. Spojakina, N.G. Kostova, I.A. Tzolovski, D.M. Shopov, Kinet. Catal. (Kinetika i Kataliz in Russian), 23 (1982) 456.
[3] A. Spojakina, S. Damyanova, D. Shopov, T.K. Shokireva, T.M. Yurieva, React. Kinet. Catal. Lett. 27 (1985) 333.
[4] A.A. Spojakina, N.G. Kostova, I.N. Yuchnovski, D.M. Shopov, T.M. Yurieva, T.K. Shokhireva, Appl. Catal. 39 (1988) 333.
[5] N.N. Tomina, A.N. Loginova, M.A. Sharikhina, Petrol. Chem. (Neftechimiya), 29 (1989) 25 (in Russian).
[6] A. Griboval, P. Blanchard, L. Gengembre, M. Fournier, J.L. Dubois, J.R. Bernard, J. Catal. 188 (1999) 102.
[7] A.A. Spojakina, N.G. Kostova, B. Sow, M.W. Stamenova, K. Jiratova, Catal. Today 65 (2001) 315.
[8] B. Pawelec, R. Mariscal, J.L.G. Fierro, A. Greenwood, P.T. Vasudevan, Appl. Catal. A: Gen. 206 (2001) 295.
[9] R. Shafi, M.R.H. Siddiqui, G.J. Hutchings1, E.G. Derouane, I.V. Kozhevnikov, Appl. Catal. A: Gen. 204 (2000) 251.
[10] A.A. Spojakina, E.U. Kraleva, K. Jiratova, J. Kocianova, L. Petrov, Bulg. Chem. Commun. 34 (2002) 495.
[11] A.A. Spojakina, K. Jiratova, N.G. Kostova, J. Kocianova, M. Stamenova, Kinet. Catal. (Kinetika i Kataliz), 44 (2003) 886 (in Russian).
[12] N.N. Tomina, A.A. Pimerzin, A.N. Loginova, M.A. Sharikhina, E.O. Shilkhina, Y.V. Eremina, Petrol. Chem. (Neftechimiya), 44 (2004) 274 (in Russian).
[13] P. Blanchard, C. Lamonier, A. Griboval, E. Payen, Appl. Catal. A.: Gen. 322 (2007) 33.
[14] L. Lizama, T. Klimova, Appl. Catal. B: Environ. 82 (2008) 139.
[15] N.N. Tomina, P.A. Nikul'shin, A.A. Pimerzin, Petrol. Chem. (Neftechimiya), 48 (2008) 92 (in Russian).
[16] A.M. Maitra, N.W. Cant, D.L. Trimm, Appl. Catal. 48 (1989) 187.
[17] C.I. Cabello, I.L. Botto, J.H. Thomas, Appl. Catal. A.: Gen. 197 (2000) 79.
[18] I. Pettiti, I.L. Botto, C.I. Cabello, S. Colonna, M. Faticanti, G. Minelli, P. Porta, J.H. Thomas, Appl. Catal. A.: Gen. 220 (2001) 113.
[19] C.I. Cabello, M. Munoz, E. Payen, H.J. Thomas, Catal. Lett. 92 (2004) 69.
[20] C.I. Cabello, M. Munoz, I.L. Botto, E. Payen, Thermochim. Acta 447 (2006) 22.
[21] N.R. Gazimzyanov, K.P. Zhdanova, V.I. Kvashonkin, Kinet. Catal. (Kinetika i Kataliz), 36 (1995) 626 (in Russian).
[22] P.A. Nikul'shin, Y.V. Eremina, N.N. Tomina, A.A. Pimerzin, Petrol. Chem. (Neftechimiya), 46 (2006) 343 (in Russian).
[23] N.N. Tomina, P.A. Nikul'shin, A.A. Pimerzin, Kinet. Catal. (Kinetika i Kataliz), 49 (2008) 653 (in Russian).
[24] C.I. Cabello, F.M. Cabrerizo, A. Alvarez, H.J. Thomas, J. Mol. Catal. A 186 (2002) 89.
[25] C. Lamonier, C. Martin, J. Mazurelle, V. Harlé, D. Guillaume, E. Payen, Appl. Catal. B 70 (2007) 548.
[26] J. Mazurelle, C. Lamonier, C. Lancelot, E. Payen, C. Pichon, D. Guillaume, Catal. Today 130 (2008) 41.
[27] M. Breysse, C. Geantet, P. Afanasiev, J. Blanchard, M. Vrinat, Catal. Today 130 (2008) 3.
[28] J.A.R. van Veen, E. Gerkema, A.M. van der Kraan, A. Knoester, J. Chem. Soc., Chem. Commun. (1987) 1684.
[29] H. Farag, I. Mochida, K. Sakanishi, Appl. Catal. A 194–195 (2000) 147.
[30] J.P.R. Vissers, F.P.M. Mercx, S.M.A. Bouwens, V.H.J. de Beer, R. Prins, J. Catal. 114 (1988) 291.
[31] C. Glasson, C. Geantet, M. Lacroix, F. Labruyere, P. Dufresne, J. Catal. 212 (2002) 76.
[32] M.T. Pope, Heteropoly and Isopoly Metallates, Springer, Berlin, 1990;
M.T. Pope, Heteropoly and Isopoly Metallates, Nauka, Novosibirsk, 1983.
[33] G. Brauer (Ed.), Handbuch der praporativen anorganischen Chemie, Ferdinand Enke, Stuttgart, 1975–1981;
G. Brauer (Ed.), Handbuch der praporativen anorganischen Chemie, Mir, Moscow, 1986.
[34] L.P. Kazanskii, A.M. Golubev, Khimiya soedinenii Mo (VI) i W(VI),(Chemistry of Mo(VI) and W(VI) Compounds), Nauka, Novosibirsk, 1979, p. 66.
[35] M. Munoz, C.I. Cabello, I.L. Botto, G. Minelli, M. Carpon, C. Lamonier, E. Payen, J. Mol. Struct. 841 (2007) 96.
[36] M.H. Alizadeh, A.R. Salimi, J. Mol. Struct.: THEOCHEM 809 (2007) 1.
[37] H.T. Evans, J.S. Showell, J. Am. Chem. Soc. 91 (1969) 3275.
[38] A. Ginestra, F. Giannetta, P. Fiorucci, Gazz. Chim. Ital. 98 (1968) 1197.
[39] H. Topsøe, B.S. Clausen, F.E. Massoth, Hydrotreating catalysis. Science and technology, in: J.R. Anderson, M. Boudart (Eds.), Catalysis – Science and Technology, vol. 11, Springer-Verlag, Berlin/Heidelberg/New York, 1996, p. 310.
[40] Y.I. Yerwakov, A.N. Startsev, V.A. Burmistrov, Appl. Catal. 11 (1984) 1.
[41] A.N. Startsev, Catal. Rev. -Sci. Eng. 37 (1995) 353.
[42] C.M.C. Romero, J.W. Thybaut, G.B. Marin, Catal. Today 130 (2008) 231.
[43] M. Breysse, E. Furimsky, S. Kasztelan, M. Lacroix, G. Perot, Catal. Rev. 44 (2002) 651.
[44] V.M. Kogan, Appl. Catal. A: Gen. 237 (2003) 161.
[45] G.V. Isagulyants, A.A. Greish, V.M. Kogan, in: M.J. Phillips, M. Ternan (Eds.), Proc. 9th Intern. Congr. Catal., vol. 1, Ottawa, Canada, (1988), p. 35.
[46] V.M. Kogan, A.A. Greish, G.V. Isagulyants, Catal. Lett. 6 (1990) 157.
[47] V.M. Kogan, N.T. Dung, V.I. Yakerson, Bull. Soc. Chim. Belg. 104 (1995) 303.
[48] V.M. Kogan, N.N. Rozhdestvenskaya, I.K. Korshevets, Appl. Catal. A: Gen. 234 (2002) 207.
[49] V.M. Kogan, R.G. Gaziev, S.W. Lee, N.N. Rozhdestvenskaya, Appl. Catal. A: Gen. 251 (2003) 187.
[50] V.M. Kogan, Transition metal sulfides. Chemistry and catalysis, in: T. Weber, R. Prins, R. van Santen (Eds.), NATO ASI Series, vol. 60, Kluwer Academic Publishers, 3. High Technology, 1998, pp. 35–271.
[51] V.M. Kogan, G.V. Isaguliants, Catal. Today 130 (2008) 243.
[52] M. Daage, R.R. Chianelli, A.F. Ruppert, Stud. Surf. Sci. Catal. 75 (1993) 571.
[53] R.R. Chianelli, M. Daage, M.J. Ledoux, Adv. Catal. 40 (1994) 177.
[54] M. Daage, R.R. Chianelli, J. Catal. 149 (2) (1994) 414.